Climate Dynamics (2019) 53:6437–6452
https://doi.org/10.1007/s00382-019-04937-4

The relationship between large volcanic eruptions in different latitudinal zones and spatial patterns of winter temperature anomalies over China

Di Sun[1,2,3] · Jingyun Zheng[1,2] · Xuezhen Zhang[1,2] · Zhixin Hao[1,2]

Received: 4 January 2019 / Accepted: 10 August 2019 / Published online: 21 August 2019

Abstract
We identified regional differences over China of winter temperature response to large volcanic eruptions with different latitudes and seasons from 1956 to 2005, and investigated atmospheric circulations for corresponding spatial patterns of winter temperature anomalies using reanalysis data and simulations by the Community Earth System Model. Both observations and simulations show that spatial patterns of winter temperature anomalies over China are related to the latitudes and seasons of the eruptions. Tropical volcanic eruptions during summer led to winter temperature decreases of 0.4–1.6 °C in eastern China due to the increase of height gradient. Winter volcanic eruptions led to extensive warming over Tibet. Following summer volcanic eruptions at low latitude, there were warm winters in eastern China because of a weak Siberian high. An anomalous southerly wind caused slight warming over most of China following winter eruptions. With the typical "trough–ridge–trough" at high latitude of the Northern Hemisphere, the winter temperature decreased in northeastern China and increased in western China following summer eruptions at mid-latitude. However, temperature generally increased after winter eruptions. For summer eruptions at high latitude, winter temperature showed a coherent decrease over northwest and east-central China due to an intensified Siberian High and East Asian trough. The widespread warming occurred over China because of the meridional circulation between 65°N and 45°N was weaker following winter volcanic eruptions.

Keywords Large volcanic eruption · Winter temperature · China · CESM

1 Introduction

As an important external forcing of the climate system, large volcanic eruptions are likely to induce regional differences in global temperature change, which have attracted widespread attention since their noticeable effects on agriculture and the social economy (e.g., Robock 2000; Cole-Dai 2010). Once such eruptions occurred, regional differences of global temperature anomalies mainly depended on the latitudes and seasons of those eruptions. The atmospheric circulation anomalies at eruption years were strongly latitudinal dependent, with effects on polar vortex and monsoon system, and both the temperatures in boreal summer and winter showed large differences when they responded to the different latitudinal eruption events. For instance, there was cooling in western America, western and central Europe, and the western Mediterranean during the cold season (October–March) following the tropical Mount Tambora eruption (8.25°S) in 1815 (Shindell et al. 2004), and the summer temperature in 1816 was normal or slightly warmer than average in eastern Europe and western Russia (Casty et al. 2007; Luterbacher and Pfister 2015). However, after the Mount Pinatubo eruption at low latitude (15.13°N) in 1991, the mid and high latitudes of the Northern Hemisphere experienced obvious cooling overall during the subsequent 1–2 summers (Groisman 1992). During winter 1991, the temperature increased in North America, Europe and most of Siberia, but decreased in Alaska, Greenland, the Middle East and China after the Mount Pinatubo eruption (Groisman 1992; Graf et al. 1993; Robock and Mao 1995; Parker

✉ Zhixin Hao
haozx@igsnrr.ac.cn

[1] Key Laboratory of Land Surface Pattern and Simulation, Institute of Geographic Sciences and Natural Resources Research, Chinese Academy of Sciences, Beijing, China

[2] University of Chinese Academy of Sciences, Beijing, China

[3] Beijing Jingshan School Chaoyang Branch School, Beijing, China

et al. 1996; Kirchner et al. 1999; Robock 2000). Moreover, Robock and Mao (1992) analyzed Northern Hemisphere winter surface temperature patterns after the 12 largest volcanic eruptions during 1883–1992, finding warming over Eurasia and North America, and cooling over the Middle East. This pattern usually occurred during the first winter after tropical eruptions, in the first or second winter after mid-latitude eruptions, and in the second winter after high-latitude eruptions. Some analyses (Shindell et al. 2004) have revealed that such temperature anomalies pattern was consistent with a dynamic shift in the Arctic Oscillation (AO) or the North Atlantic Oscillation (NAO). Following large tropical volcanic eruptions, the volcanic aerosols heat the top layer of the stratosphere, enhancing the pole-to-equator gradient and leading to the trend in the strength of the polar vortex. Then the strengthened westerly winds in the lowermost stratosphere propagated down into the troposphere by interactions with planetary waves, and the enhanced surface westerlies create the typical AO spatial pattern and the broad warming over northern Europe and Russia (Shindell et al. 2004). However, using tree-ring proxy data over the past nine centuries, the regional temperature patterns were different in responses of Mount Tambora eruption from the reconstruction and Pinatubo eruption from observation data. The strongest cooling occurred during the second summer in Northern Europe, with weak cooling during the first summer in central Europe (Esper et al. 2013). In addition, simulations of volcanic eruptions at high latitude have shown that a summer eruption caused more detectable climate effects than those in other seasons. It may be an ideal or near-ideal combination of aerosol formation rate, deposition and insolation, which lead to the largest reduction of radiative forcing after the summer eruptions (Kravitz and Robock 2011). In addition, the season of eruption occurrence was also a crucial factor to affect temperature responses. For example, the boreal winter temperature decreased significantly over the Asian continent and North America after april eruptions due to the land surface feedbacks. The reverse temperature responses occurred following october eruptions, which was likely a result of sea ice and associated feedbacks (Stevenson et al. 2017).

As a vast country in eastern Asia, China has large spatial and temporal differences in climate variability, which are regulated by climate forcing, such as solar cycle and large volcanic eruptions (e.g., Chen and Zhou 2012; Zhou et al. 2013; Miao et al. 2016). Using observational and satellite data, some studies have shown that spatial patterns of temperature across the country have a close relationship with large volcanic eruptions in various latitudinal zones. For example, there was widespread cooling over China in the summer–autumn of 1992 after the low-latitude Mount Pinatubo eruption. In particular, summer temperature dramatically decreased by 3–5 °C over the Yangtze River valley (Xu 1995). Furthermore, there was drastic cooling of summer temperature in north of the Yangtze river valley after the Mount St. Helens eruption at mid-latitude (46.11°N) in 1980 (Xu 1986). According to historical documents, a cold summer in 1601 over the middle and lower reaches of the Yangtze Valley was recorded following the Mount Huaynaputina eruption in the Southern Hemisphere (16.36°S) in 1600 (Fei and Zhang 2008). Based on the records in the local chronicles of the Ming and Qing dynasties, the cooling occurred in the summer of 1601 when abnormally snow event appeared in the lower reaches of the Yangtze River. Moreover, using the ice core in Greenland, the start year of Mount Eldgjá eruption at high latitude (63.58°N) was identified at 934 and the eruption probably continued 3–8 years. Following the Mount Eldgjá eruption, the cooling over the Northern Hemisphere mainly appeared in 935 and 939–940, in the meantime, an abrupt cooling in central China and freezing canals in the lower reaches of the Yangtze River occurred in winter of 939. (Fei and Zhou 2006).

Although some studies have addressed the climate effect of several famous volcanic eruptions in the 20th century on temperature changes in China (Jia and Shi 2001), very few works pay attention to regional differences of temperature changes over China which caused by latitudinal and season factors of volcanic eruptions. In addition, possible relationships between large volcanic eruptions and regional temperature response have not been fully addressed. Therefore, the goal of this study was to identify which volcanic eruption (including locations and seasons) had major impacts on winter temperature anomalies over China, and to fully map the spatial patterns of those anomalies after the eruptions. Furthermore, causes of spatial differences in the anomalies were analyzed using China meteorological administration (CMA) gridded reanalysis data and sensitivity experiments by the community Earth system model (CESM).

2 Data and methods

2.1 Data

A 0.5°×0.5° gridded monthly temperature dataset for the period 1951–2010 was made available by the CMA (http://data.cma.cn/data/cdcdetail/dataCode/SEVP_CLI_CHN_TEM_MON_GRID.html). This dataset was generated from the following four components: monthly mean temperature series of national basic and referenced climatological stations for 1951–2004; a monthly surface temperature dataset for 2005–2010; global gridded climate dataset from the National Climatic Data Center; a gridded temperature dataset (1°×1°) of China from digital elevation model of GTOPO30 (https://www.usgs.gov/centers/eros/science/

usgs-eros-archive-digital-elevation-global-30-arc-second-elevation-gtopo30).

Three volcanic datasets were used in this study. The first is a chronology of large volcanic eruptions from the Smithsonian institution (http://volcano.si.edu/search_eruption.cfm), including longitude and latitude, altitude, starting and ending dates of volcanic eruptions and the volcanic explosivity index (hereafter, VEI). Due to the limited historical records, one kind of index sequence should be introduced to show volcanic aerosol changes with different magnitudes. Although sometimes VEI could not reflect the stratospheric sulfur injection, for example, the VEI 5 eruption of the 1980 Mount St. Helens had the measurable climatic impact (Newhall et al. 2018), it presents intensity of the volcanic eruptions. In addition, the VEI positively correlated with dust veil index (DVI) and ice core volcanic index (IVI) for most volcanic eruption events (Robock and Free 1996). Thus, the VEI was selected to estimate of explosive magnitude for historical volcanism. Based on the chronology, there are 29 large volcanic eruptions (VEI ≥ 4) from 1956 to 2005. When compared temperature changes before and after volcanic eruptions, eruptions prior to 1956 were not considered because instrumental temperature data began in 1951. The numbers of large volcanic eruptions in tropical regions (10°S–15°N), low–mid latitude (15°N–50°N), and high latitude (50°N–90°N) were 14, 5 and 10, respectively (Table 1). The second dataset was the volcanic aerosol mass mixing ratio data prototype provided by the National Center for Atmospheric Research (NCAR). It includes monthly stratospheric aerosol distributions for volcanic eruptions since 1860. The dataset has been customized by CESM grid cells to accurately prescribe stratospheric aerosols in simulation (Neely et al. 2016). This was used for identifying the time series of the global mean mass mixing ratio of volcanic dust following eruptions since 1850. The third dataset was the (IVI) reconstructed by ice core records from the Arctic and Antarctica (Gao et al. 2008). It consists of monthly gridded volcanic aerosol mass mixing ratios over the past 1500 years, and was used to calculate the relationships of the global volcanic aerosol mass mixing ratio between eruptions of VEI 4, 5 and 7.

The 2.0° × 2.0° gridded reanalysis data from 1851 to 2014 were derived from NOAA-CIRES 20th Century reanalysis dataset (V2c) provided by NOAA's Earth System Research Laboratory Physical Sciences Division (http://www.esrl.noaa.gov/psd/data/gridded/data.20thC_ReanV2c.html). The sea level pressure data and geopotential heights data which include 24 pressure levels were used in this study.

2.2 Method and Design of Experiment

Some studies found that El Niño response was associated with the intensity of volcanic eruptions (Lim et al. 2015; Predybaylo et al. 2017). There was a threshold of the volcanic forcing to leading the El Niño events. However, the intensity of most volcanic eruptions in this study was only VEI 4. Therefore, the possible link between volcanic eruptions and El Nino events was ignored when we identified the effect of volcanic eruptions. In addition, we focus on the underlying effects on temperature within 10-year after large volcanic eruptions. Since ENSO was the mainly internal mode that affected the temperature changes in subsequent 10 years, it needs to minimize the influence of ENSO. In this study, the influence of ENSO in the observational data was removed using a linear regression method: $y' = y - r$ (CTI, y) × CTI (Iles et al. 2013), where y' is ENSO-independent temperature anomaly series and r is the regression coefficient of winter ENSO index-cold tongue index (CTI) onto temperature series. The cold tongue index was defined as the average SST anomaly over 6°N–6°S, 180°–90°W, minus the global mean SST (http://research.jisao.washington.edu/

Table 1 Twenty-nine large volcanic eruptions since 1956 as recorded in Smithsonian Institution chronology

No	Year/Month	Name	VEI	Latitude
1	1956/03	Bezymianny	5	55.98°N
2	1963/03	Agung	5	8.34°S
3	1963/05	Agung	5	8.34°S
4	1964/11	Shiveluch	4	56.65°N
5	1965/09	Taal	4	14.00°N
6	1966/04	Kelut	4	7.93°S
7	1966/08	Awu	4	3.67°N
8	1968/06	Fernandina	4	0.37°S
9	1973/07	Chachadake	4	44.35°N
10	1974/10	Fuego	4	14.47°N
11	1975/07	Tolbachik	4	55.83°N
12	1976/01	Augustine	4	59.36°N
13	1980/05	St. Helens	5	46.20°N
14	1981/04	Alaid	4	50.86°N
15	1981/05	Pagan	4	18.13°N
16	1982/04	El Chichón	4	17.36°N
17	1982/05	Galunggung	4	7.25°S
18	1983/07	Colo	4	0.17°S
19	1986/03	Augustine	4	59.36°N
20	1986/11	Chikurachki	4	50.33°N
21	1990/01	Kliuchevskoi	4	56.06°N
22	1990/02	Kelut	4	7.93°S
23	1991/06	Pinatubo	6	15.13°N
24	1992/06	Spurr	5	61.30°N
25	1994/09	Rabaul	4	4.27°S
26	2000/09	Ulawun	4	5.05°S
27	2001/05	Shiveluch	4	56.65°N
28	2002/09	Ruang	4	2.30°N
29	2002/11	Reventador	4	0.08°S

data/cti/). Based on the filtered temperature anomaly series, temperature differences between two winters following volcanic eruptions and five winters prior to eruptions were calculated on each grid to generate spatial patterns of winter temperature for 29 eruptions since 1956 in Table 1. China was divided into five sub-regions (i.e. northeast, east-central, southeast, northwest and Tibet) which refer to the division by Ge et al. (2010). Thus, the spatial patterns for representative large eruptions were used to show regional differences of winter temperature over China. The representative eruptions were firstly chosen based on VEI which was greater than or equal to five in each latitudinal zone. In tropical latitude, only eruption of Mount Agung reached VEI 5. Both Mount Pinatubo and St. Helens reached VEI 5 in low–mid latitude. Although the Mount Bezymianny and Spurr reached VEI 5 in high latitude, the eruption of Mount Bezymianny was in El Niño phase and the eruption of Mount Spurr was in La Niña phase (https://www.cpc.ncep.noaa.gov/products/analysis_monitoring/ensostuff/ensoyears_1971-2000_climo.shtml), which may confuse the effects of volcanic eruption. Thus, Mount Shiveluch was chosen as the latest large volcanic eruption in high latitude. Moreover, Mount El Chichón also was chosen as the sample eruption due to its strong social and economic impacts around the world. Finally, five eruptions of Mount Agung, St. Helens, El Chichón, Pinatubo, and Shiveluch were selected to show the temperature responses to large volcanic eruptions. Then, for volcanic eruptions in the same latitudinal zone, similar temperature patterns were classified into a group by hierarchical cluster analysis of all temperature patterns after volcanic eruptions in this latitudinal zone. The mean spatial pattern for one group was regarded as the spatial temperature response in China after eruptions at one certain latitude. The significance test was used to indicate where the temperature anomalies exceeded one standard deviation, and the standard deviation was calculated using winter temperature for the period 1951-1990 (Ottera 2008).

All simulations were performed by the CESM (Hurrell et al. 2013). The model consists of the community atmosphere model version 4, parallel ocean program version 2, community land model version 4 (CLM4), and Community Ice Code version 4 (CICE4), the Land-Ice Component and the Coupler. In our study, all components were active except for the C–N cycle in CLM4. A 1250-year control simulation and 10-year sensitivity experiments were performed. The control experiment was forced with constant preindustrial external forcing, including total solar irradiation of 1360 Wm^{-2}, CO_2 concentration of 284.7 ppmv, CH_4 concentration of 791.6 ppbv, N_2O concentration of 275.7 ppbv, and land use and land cover for 1850. The control run provided initial conditions for the sensitivity experiments. The performances of CESM have been extensively discussed in a special issue of the Journal of Climate (http://journals.ametsoc.org/topic/ccsm4-cesm1, last access: June 2017). As demonstrated by many studies (e.g., Landrum et al. 2013; Lehner et al. 2015), the CESM well reproduced temperature characteristics revealed by historical and proxy-data records. For example, CESM could capture the warm Medieval Climate Anomaly (MCA, 950–1250 CE) and a transition into the Little Ice Age (LIA, 1400–1700 CE), which was in reasonable agreement with both reconstructions and other models. In addition, CESM also showed adequate performance in simulating the direct and indirect effects of aerosols on the climate system (Lamarque et al. 2012). Compared with satellite and surface measurement datasets, the CAM4-chem of CESM was approved to represent the chemistry of the troposphere and the stratosphere. The cooling amplitude simulated by CESM for the Mount Pinatubo eruption was generally agreed with that of the observations (Lehner et al. 2015). The 1000-year control run well simulated the variability of East Asian summer monsoon and summer precipitation over eastern China, which has been demonstrated by other studies (Zheng et al. 2017; Zhang et al. 2018).

Our sensitivity experiments were used to identify how external forcing drove winter temperature responses and analyze the effects of volcanic forcings in different latitudinal zones. The sensitivity experiments were set up as branch runs from the control experiment, and all forcings were the same as the control experiment except for the volcanic forcing. We performed eight sensitivity experiments, i.e., four eruptions at tropical (10°S–10°N), low (10°N–30°N), mid (30°N–60°N) and high (60°N–90°N) latitudes, and during two seasons (summer half-year of may–september and winter half-year of october–april). The intensities of the volcanic forcings for eight sensitivity experiments were VEI 4, thus, the differences between them were from their latitudinal locations and eruption seasons. To reduce model noise, a five-member ensemble mean for each set of sensitivity experiment was calculated to represent spatial patterns of winter temperature response over China, which could reduce the internal variability of the climate system and highlight the influence signals from external forcing. The student *t* test was used to show the significance for each ensemble mean.

In the NCAR dataset, 14 volcanic eruptions could be clearly identified around the world in the series of global mean mass mixing ratio of volcanic dust during the past 150 years. Then, as shown in Table 2, the eruptions with maximum intensity in each latitudinal zone and season were selected as the sample eruption. The NCAR dataset did not have records of winter eruptions at high latitude. Thus, temporal and magnitude changes of volcanic aerosol mass mixing ratios for those eruptions were referred to that of Mount Spurr (high latitude in summer). To simulate eruptions for different latitudes and seasons with the same intensity, volcanic aerosol mass mixing ratios (hereafter, VMR) for the four latitude zones (tropical, low, mid and high) and two seasons (summer and winter

Table 2 Large volcanic eruptions in four latitudinal zones since 1850 from the NCAR dataset

Volcano name	VEI	Latitude	Latitude zone	Year/month	Summer/ winter half year
Krakatau	6	6.10°S	Tropical	1883/08	Summer
Agung	5	8.34°S	Tropical	1963/03	Winter
Pinatubo	6	15.13°N	Low	1991/06	Summer
Santa María	6	14.76°N	Low	1902/10	Winter
Novarupta	6	58.27°N	Mid	1912/06	Summer
Shiveluch	5	56.65°N	Mid	1854/02	Winter
Spurr	4	61.30°N	High	1953/07	Summer

half-years) were constructed by rescaling the VMR at each grid cell of seven VMR sample series from the NCAR dataset (Table 2). The rescaling factor depends on VMR multiples of large eruptions with VEIs 4, 5 and 7 from the IVI dataset. Therefore, using the existing relationship between volcanic intensity and time (VMR = $F(t)$), the series of volcanic eruptions of any intensity was calculated as follows:

$$\mathrm{VMR} = F(S_1 \times t) \times S_2 \tag{1}$$

$$\text{where, } S_1 = \frac{T_0}{T_x}$$

$$\text{and, } S_2 = \frac{M_x}{M_0}.$$

Variables S_1 and S_2 denote the temporal rescale and amplitude rescale factors, respectively. T_0 and T_x denote the duration between the VMR peak to approximately zero. Variables M_0 and Mx denote the total global VMR. The subscript 0 represents the sample eruption (i.e., the identified volcanic eruptions in Table 2). The subscript x refers to the mean value of the sample eruption derived from the IVI dataset.

Figure 1 shows volcanic forcings with different latitudes and seasons using the above method. The experiments aim to study the effects of volcanic eruptions on winter temperatures over China. Specifically, we focused on the dependence of these effects on eruption locations and seasons. Therefore, all sensitivity experiments were classified into eight subgroups, which were identified by four eruption latitudes and two eruption seasons. The differences among these subgroups generally resulted from various eruption latitudes and seasons. The VMRs were zero before volcanic eruptions, it increased quickly and reached the maximum value at the fifth month after eruptions. Since the volcanic aerosols from different locations had distinctive meridional distributions, the volcanic aerosols of tropical and low latitudes eruptions expanded poleward quickly, and were detectable in third and second year following summer eruption and winter eruption, respectively. The decay process of volcanic aerosols from eruptions at low latitude was similar to that of tropical eruptions. However, the volcanic aerosols in mid and high latitudes only stayed at the Northern Hemisphere and did not transport to the Southern Hemisphere. The aerosols of above two eruptions stayed in the stratosphere for about two years.

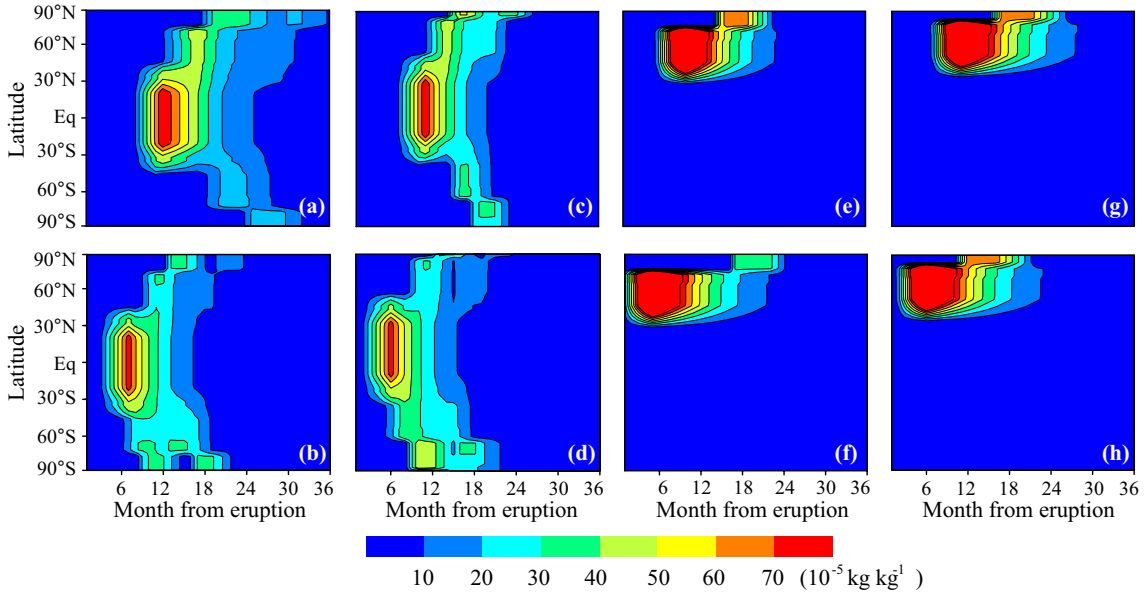

Fig. 1 Meridional distributions of zonally-averaged, monthly volcanic aerosols at tropical (**a**, **b**), low (**c**, **d**), mid (**e**, **f**), and high (**g**, **h**) latitudes in summer half-year (**a**, **c**, **e**, **g**) and winter half-year (**b**, **d**, **f**, **h**). Zero in the x-axis denotes the month when large volcano erupted

3 Results

3.1 Spatial pattern of winter temperature over China after large volcanic eruptions at different latitudinal zones

Table 3 shows information of several large volcanic eruptions with different latitudes and seasons since 1950, and Fig. 2 presents corresponding mean patterns of winter temperature in China during the subsequent two winters. The eruptions of Mount Agung, which occurred in spring at tropical latitudinal zone, caused winter temperature decrease over eastern China (east of 105°E), with strong cooling over the northeast. Western China (west of 105°E) experienced a warm winter following the eruption (Fig. 2a). Although the eruption of Mount El Chichón also occurred during spring, the location of volcano was in the low-mid latitudinal zone, which caused different winter temperature responses compared to the eruption of Mount Agung. The significant cooling appeared over most regions of China, especially in the southeast with the temperature decreased more than 2.0 °C (Fig. 2c). Compared with the Agung and El Chichón eruptions, the warming area extended northward after the summer eruptions of Mount St. Helens and Pinatubo at low-mid latitude. The winter temperature increased over the northeast and northwest (Fig. 2b and d). Further, the temperature over eastern Tibet was dropped by 0.8–1.6 °C after the eruption of Mount Pinatubo (Fig. 2d). In addition, after the summer eruption of Mount Shiveluch at high latitudinal zone, winter temperature increased by 2.0 °C over the northeast and Tibet, and slightly decreased by 0.4–0.8 °C over northwestern China (Fig. 2e). Comparing spatial patterns following many large volcanic eruptions, it illustrated that regional differences in winter temperature not only depend on eruption locations but also their seasons.

To reveal the relationship between the latitude of volcanic eruptions and the spatial pattern of winter temperature in China, the eruptions were divided into three groups according to the latitude. As shown in Table 4, the regional temperature response to 29 volcanic eruptions since 1956 was strongly associated with their latitudes and seasons. Further, Fig. 3 shows ensemble mean spatial patterns of temperature for each group of eruptions in Table 4. Following 14 tropical eruptions, ten led to the first spatial pattern, in which the temperature increased by 0.4–1.6 °C over Tibet and decreased by 0.4–2.0 °C in eastern China. In particular, the cooling magnitude was more than 1.2 °C over the northeast and northwest (Fig. 3a). Among ten eruptions, seven were in spring and summer (march–august). In contrast, the other four eruptions, which were all in autumn and winter (september–february), led to widespread warming across the northeast and Tibet. The temperature increased by 0.4–1.2 °C over the northeast while strong cooling of 0.4–1.6 °C occurred in southeast and Tibet (Fig. 3b).

After five volcanic eruptions at low-mid latitude, two led to cooling in east-central and southeast and warming in

Table 3 Information of five volcanic eruptions since 1956

Volcano name	VEI	Latitude	Latitude zone	Year/month	Season
Agung	5	8.34°S	Tropical	1963/03	Spring
St. Helens	5	46.20°N	Low-mid	1980/05	Summer
El Chichón	4	17.36°N	Low-mid	1982/04	Spring
Pinatubo	6	15.13°N	Low-mid	1991/06	Summer
Shiveluch	4	56.65°N	High	2001/05	Summer

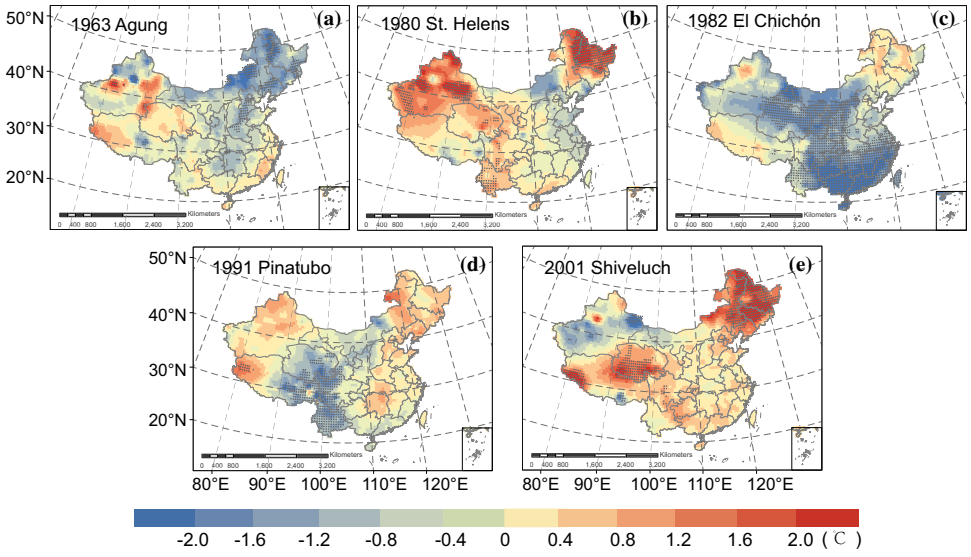

Fig. 2 Spatial patterns of winter temperature anomalies between two post-volcanic winters and five previous-volcanic winters in China after eruptions of Agung (**a**), St. Helens (**b**), El Chichón (**c**), Pinatubo (**d**) and Shiveluch (**e**). Dots indicate the confidence areas exceeding one standard deviation

Table 4 Classification of volcanic eruptions in three latitude zones, which led to two spatial patterns of winter temperature in China

	First spatial pattern		Second spatial pattern	
	Volcano name	Year/month	Volcano name	Year/month
Tropical latitude (10°S–15°N)	Agung	1963/03	Fuego	1974/10
	Agung	1963/05	Kelut	1990/02
	Taal	1965/09	Rabaul	1994/09
	Kelut	1966/04	Ulawun	2000/09
	Awu	1966/08		
	Fernandina	1968/06		
	Galunggung	1982/05		
	Colo	1983/07		
	Ruang	2002/09		
	Reventador	2002/11		
Low-mid latitude (15°N–50°N)	Mount St. Helens	1980/05	Chachadake	1973/07
	El Chichón	1982/04	Pagan	1981/05
			Pinatubo	1991/06
High latitude (50°N–90°N)	Bezymianny	1956/03	Shiveluch	1964/11
	Augustine	1986/03	Tolbachik	1975/07
	Chikurachki	1986/11	Augustine	1976/01
	Shiveluch	2001/05	Alaid	1981/04
			Kliuchevskoi	1990/01
			Spurr	1992/06

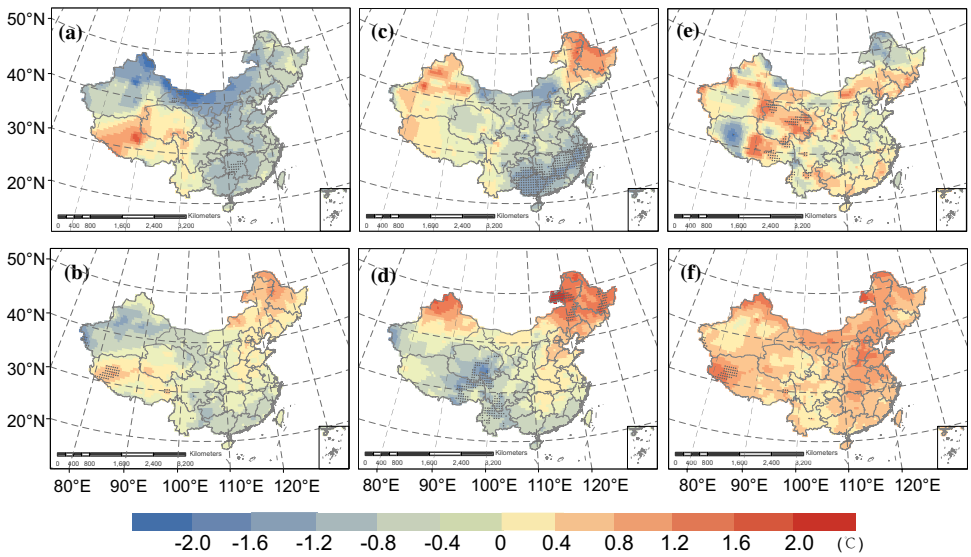

Fig. 3 Spatial patterns of winter temperature anomalies between two post-volcanic winters and five previous-volcanic winters in China after large volcanic eruptions at tropical (**a**: first pattern, **b**: second pattern), low-mid (**c**: first pattern, **d**: second pattern), and high (**e**: first pattern, **f**: second pattern) latitudes from 1956 to 2005. Dots indicate the confidence areas exceeding one standard deviation

northeast and northwest. The temperature decrease reached 1.2 °C over the east-central, and exceeded 1.6 °C in the southeast. The temperature increased by 0.4–1.2 °C over northeast and northwest (Fig. 3c). The second spatial pattern resulting from the other three volcanic eruptions was quite opposite. Obvious warming appeared over the northern parts of the northwest and northeast, and the slight warming occurred in the east-central area. The cooling areas located in Tibet and southern parts of southeast China (Fig. 3d). Although only five large volcanic eruptions occurred at low-mid latitude during 1956–2005, the effect of volcanic season on the spatial pattern of winter temperature in China could also be identified. Two eruptions that led to the first spatial pattern of winter temperature both occurred in spring, while the other eruptions that caused the second spatial pattern all occurred in summer.

Winter temperature over China had notable spatial differences following four of ten large volcanic eruptions at high latitude. Southeast, northwest and eastern parts of Tibet experienced a warmer winter, with temperature increased by about 0.4 °C, 0.8 °C and 0.8 °C, respectively. Whereas, the east-central occurred slight cooling with approximately 0.4 °C (Fig. 3e). The other six large volcanic eruptions at high latitude led to widespread warming in China (Fig. 3f). The volcanic season also affected regional winter temperature responses. Eruptions in spring (three of the total four

eruptions) caused the first spatial pattern (Fig. 3e), consistent with the results of eruptions in the other two latitudinal zones. However, the seasons of eruptions that caused the second spatial pattern were very different. This may be because the numbers of eruptions were limited.

Compared with the spatial temperature pattern after typical five volcanic eruptions (Fig. 2) and mean temperature pattern for volcanic eruptions in different latitudinal zones (Fig. 3), the temperature patterns were similar following volcanic eruptions with same latitudinal location and seasons. For example, the spatial temperature pattern of Mount Agung (Fig. 2a) was similar to the corresponding mean temperature pattern of tropical eruptions (Fig. 3a). The eruption of Mount Pinatubo led to warming in northeast and cooling in eastern Tibetan Plateau (Fig. 2d), which was consistent with the corresponding mean temperature pattern of summer eruptions in low-mid latitude (Fig. 3d). Therefore, spatial temperature responses of the typical volcanic eruptions agreed well with the ensemble spatial pattern of winter temperature over China after large volcanic eruptions at different latitudinal zones.

Overall, the winter temperature responses exhibited regional differences following volcanic eruptions at different latitudes and seasons. For eastern China, the temperature strongly decreased over east-central and southeast following spring and summer eruptions in tropical zone and spring eruptions at low-mid latitude, it increased dramatically over northeast during the other seasons. For western China, the temperature responses were more complex compared with those over eastern China. Anomalous warming over the northwest appeared after eruptions at high latitude, and there was serious cooling in Tibet after summer eruptions at low-mid latitude.

3.2 Relationship between spatial patterns of winter temperature over China and changes of atmospheric circulation after large volcanic eruptions

Changes of winter temperature over China are closely associated with the East Asian winter monsoon (Gong et al. 2001; Huang et al. 2007; Wang and Chen 2010). Therefore, we investigated the effects of volcanic eruption latitude on the spatial winter temperature pattern over China by analyzing atmospheric circulations at 500 hPa level and sea level pressure (SLP). The 500 hPa atmospheric circulation pattern after tropical eruptions, corresponding to the first spatial pattern of temperature (Fig. 3a), showed positive geopotential height anomalies extending from the Arctic to West Siberian Plain. Negative geopotential height anomalies appeared over Lake Baikal to the North Pacific. The East Asian trough intensified. Such changes caused the pressure difference between Arctic and mid-latitude was smaller than normal, and the AO was in the negative phase. This was favorable to transport cold air to Mongolia, the Hetao Plain, and the middle and lower reaches of the Yangtze river (Fig. 4a). On the surface, both the Aleutian low over the Bering Strait and Siberian high were enhanced after tropical eruptions in spring and summer. The center of the Siberian High was over Lake Baikal and its centric intensity reached 1040 hPa. Meanwhile, there was a meridional low-pressure belt from Mongolia to Tibet, which generated a pressure gradient, stronger in southeast China and weaker in northwest China, associated with the strong Siberian high. The pressure gradient led the cold air southward, and cooling the most regions of China (Fig. 5a).

The atmospheric circulation corresponding to the second spatial pattern of temperature showed the low-pressure center of the polar vortex located at Bering Strait. Positive geopotential height anomalies covered the Eurasian continent, which resulted in geopotential height anomalies at high latitude were weaker than those at mid-latitude and caused a positive phase of the AO. In particular, a positive geopotential height anomaly from the Sea of Okhotsk to North China could cut off the path of cold air from Siberia to eastern China (Fig. 4b). Although the Aleutian low significantly intensified, the Siberian high expanded from the Siberian plains to Tibet and the Indian Peninsula. The strong high-pressure system controlled over Central and East Asia, and weakened the cold air activity, so there was a warm winter in northeastern China (Fig. 5b).

After St.Helens and El Chichón eruptions at middle latitude, geopotential height anomalies from western Eurasia to eastern Eurasia were negative, positive and negative, respectively, producing a circulation pattern of "trough–ridge–trough". A positive phase of the AO occurred as low anomaly over Greenland and high anomalies over North America, North Atlantic Ocean, and Siberian plain. The blocking high over Lake Baikal extended southward to Lake Balkhash. This powerful blocking high obstructed the southward flow of cold air to China and led to warming in western China (Fig. 4c). In addition, the anomalous Siberian High expanded southward to Mongolia and northwestern China. SLP decreased simultaneously over the North Pacific. Thus, the pressure expressed as higher in the Eurasian continent and lower in the North Pacific, which associated closely with the west wind anomaly and cooling over China (Fig. 5c).

The other three eruptions at low-mid latitude caused the negative geopotential height anomaly over Greenland and positive geopotential height anomalies over Lake Balkhash and North Atlantic Ocean, which jointly led to the positive phase of the AO and obstructed meridional cold air transport from Mongolia to North China. As a consequence, a warm winter appeared over northeast and northwest. Meanwhile, an intensified southern trough generated a low vortex

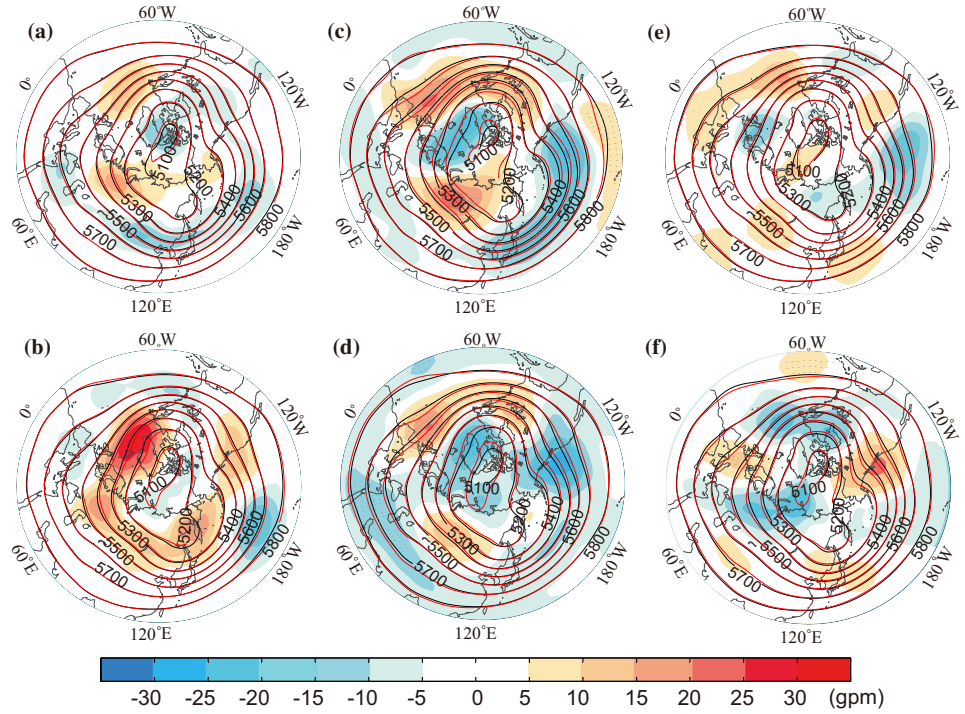

Fig. 4 Ensemble mean geopotential heights in 500 hPa of different volcanic forcings by observational data. The differences (shaded areas) were shown between two post-volcanic winters (red line) following large volcanic eruptions at tropical (**a**: first pattern, **b**: second pattern) low-mid (**c**: first pattern, **d**: second pattern), and high (**e**: first pattern, **f**: second pattern) latitudes from 1956 to 2005, with corresponding five previous-volcanic winters (black line). Dots indicate the confidence areas exceeding one standard deviation

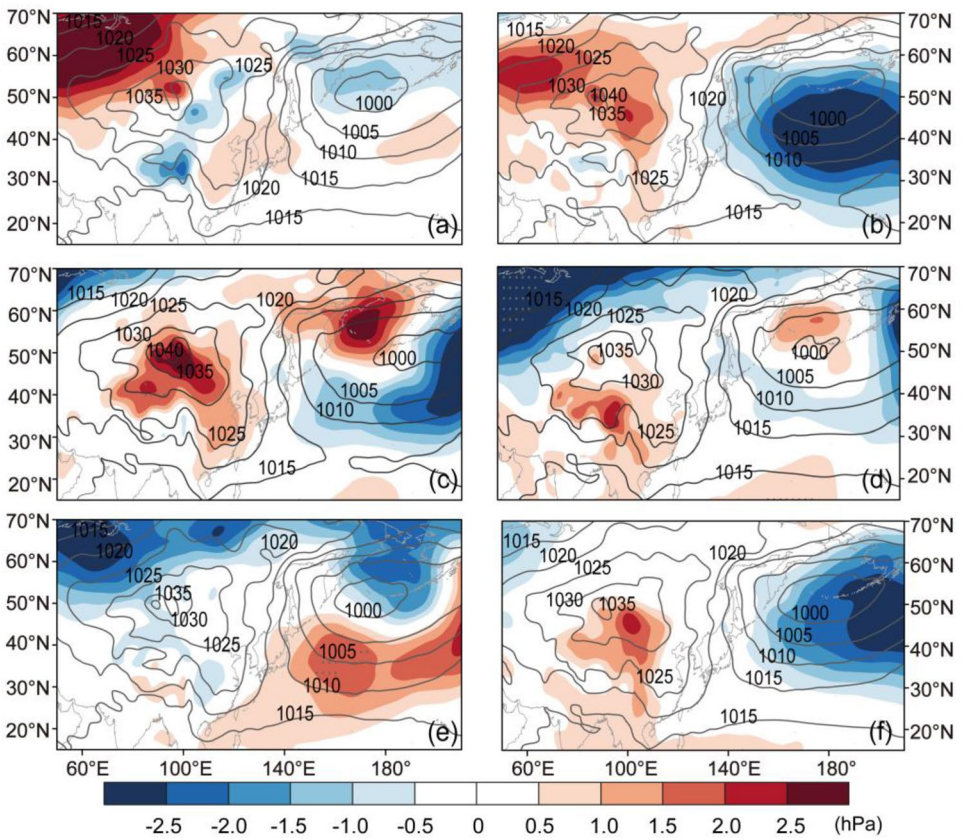

Fig. 5 Ensemble mean sea level pressure patterns of different volcanic forcings by observational data. The differences (shaded areas) were shown between two post-volcanic winters (black line) following large volcanic eruptions at tropical (**a**: first pattern, **b**: second pattern), low-mid (**c**: first pattern, **d**: second pattern), and high (**e**: first pattern, **f**: second pattern) latitudes from 1956 to 2005, with differences relative to five previous-volcanic winters. Dots indicate the confidence areas exceeding one standard deviation

over the Bay of Bengal to Tibet, which favored cooling in Tibet and southeastern China (Fig. 4d). The changes of SLP well corresponded to the geopotential height anomalies at 500 hPa. The cold air was blocked in the polar region by the weak Siberian High and Aleutian Low. Because Tibet was a cold source in winter, the divergence of cold air over the

plateau was responsible for cooling across Tibet and southeast China (Fig. 5d).

The changes of geopotential height anomalies were slight after volcanic eruptions at high latitude. The geopotential height was higher than normal years around Lake Baikal and the eastern coast of the Asian continent, where the high-pressure ridge was intensified and the East Asian trough was weakened. Conversely, the geopotential height was lower over the Bering Strait. The negative anomaly in the Arctic and positive anomaly in the mid-latitude exhibited a structure typical of the positive phase of the AO, thus prevented the cold air southward (Fig. 4e). Furthermore, SLP decreased from the Arctic Ocean to subarctic ocean, the Siberian High was weak, and the SLP increased over the North Pacific. Such a pressure gradient was associated with the southerly wind and warm winter in China (Fig. 5e).

In the second spatial pattern of atmospheric circulation at 500 hPa, a negative geopotential height anomaly was prominent from the Ural mountains to the east of Lake Baikal, with positive anomalies on its east and west sides. The AO was in a positive phase due to the increased pressure difference between the Arctic and mid-latitude. Thus, the East Asian trough was weak slightly. The cold air remained at high latitude with weak meridional circulation, so winter temperature increased over most of China (Fig. 4f). Meanwhile, there was a major positive anomaly over Tibet. Together with the weak Siberian High, the pressure anomaly was weaker in the North Pacific, which did not favor cold air transport (Fig. 5f).

Generally, cooling over eastern China could attribute to development of the East Asian trough and a high-pressure ridge near Lake Baikal. Moreover, decrease of winter temperature in Tibet was dependent on the southern trough after large eruptions at tropical and low-mid latitudes. Cold air was induced by intensified zonal circulations after eruptions at high latitude.

3.3 The simulated spatial patterns of winter temperature over China and changes of atmospheric circulation after large volcanic eruptions by CESM

Some simulations have found that the climate responses to large volcanic eruptions were closely related to the location of volcanoes. For instance, the volcanic eruptions were classified into three types based on their meridional aerosol distributions: the northern hemisphere (NH) eruptions, tropical eruptions and the southern hemisphere (SH) eruptions. The global monsoon precipitation in one hemisphere is enhanced significantly when volcanic eruptions occurred in the other hemisphere. The NH monsoon precipitation was less after tropical eruptions than that after NH eruptions (Liu et al. 2016). In addition, an El Niño-like response exists after the NH eruptions and tropical eruptions and a La Niña-like response appeared after SH eruptions (Stevenson et al. 2016; Liu et al. 2018). Besides, a large number of studies have focused on the climate effects from large volcanic eruptions at tropical or high latitudes over the Northern Hemisphere (Oman et al. 2005; Fischer et al. 2007; Schneider et al. 2009). However, little researches paid attention to the climate response to eruptions at mid-latitude. Limited by the time scale of instrumental data, there are very few mid-latitude large eruptions. Only five eruptions occurred at low–mid latitude (15°N–50°N) during 1956–2005. Thus, simulations were run using a more detailed division of low–mid latitude, i.e., four latitudinal zones were specified. These were tropical (10°S–10°N), low (10°N–30°N), mid (30°N–60°N), and high (60°N–90°N). Moreover, seasons were specified according to characteristics of the monsoon (Chang et al. 2004; Wang 2006), i.e., summer half-year (may–september) and winter half-year (october–next april).

Figure 6 shows winter temperature spatial patterns in China after large volcanic eruptions by CESM. Changes of winter temperature over China had large spatial variability for eruptions during the summer half-year. There was obvious cooling over Tibet after eruptions at tropical and low latitudes, with the temperature decreasing 2 °C (Fig. 6a and c). A 0.5–1.0 °C warming was produced over northeast and southeastern China after eruptions at low latitude (Fig. 6c). However, cooling was weak after eruptions at mid-latitude, with only a 1 °C decrease in northeastern China (Fig. 6e). Following volcanic eruptions at high latitude, winter temperature generally decreased over China except for Tibet. The cooling amplitude was 2.5 °C over northeast and northwest, and the increased temperature was 0.5–1.5 °C over northern and eastern Tibet (Fig. 6g). When large eruptions occurred during the winter half-year in different latitudinal zones, winter temperature changes were similar over subregions of China. Tropical eruptions in the winter half-year caused a temperature decrease of 0.5–1.5 °C over northeast and southeast. While winter temperature increased in the other three regions, particularly, the warming amplitude was more than 2.5 °C in eastern parts of Tibet (Fig. 6b). This was opposite that of tropical eruptions in the summer half-year. Winter temperature in China increased 0.5–2.0 °C after eruptions at low and mid latitudes. Slight cooling occurred in the southeast China after eruptions at low latitude, and in the northeast and southeast China after eruptions at mid-latitude (Fig. 6d and f). Except for slight cooling in western Tibet, the temperature increased over most of China after eruptions at high latitude, especially in northern China (Fig. 6h).

Above simulated temperature patterns for volcanic eruptions in different latitudinal zones well corresponded to mean temperature pattern using observational data. For instance, both observational analysis and simulations indicated that

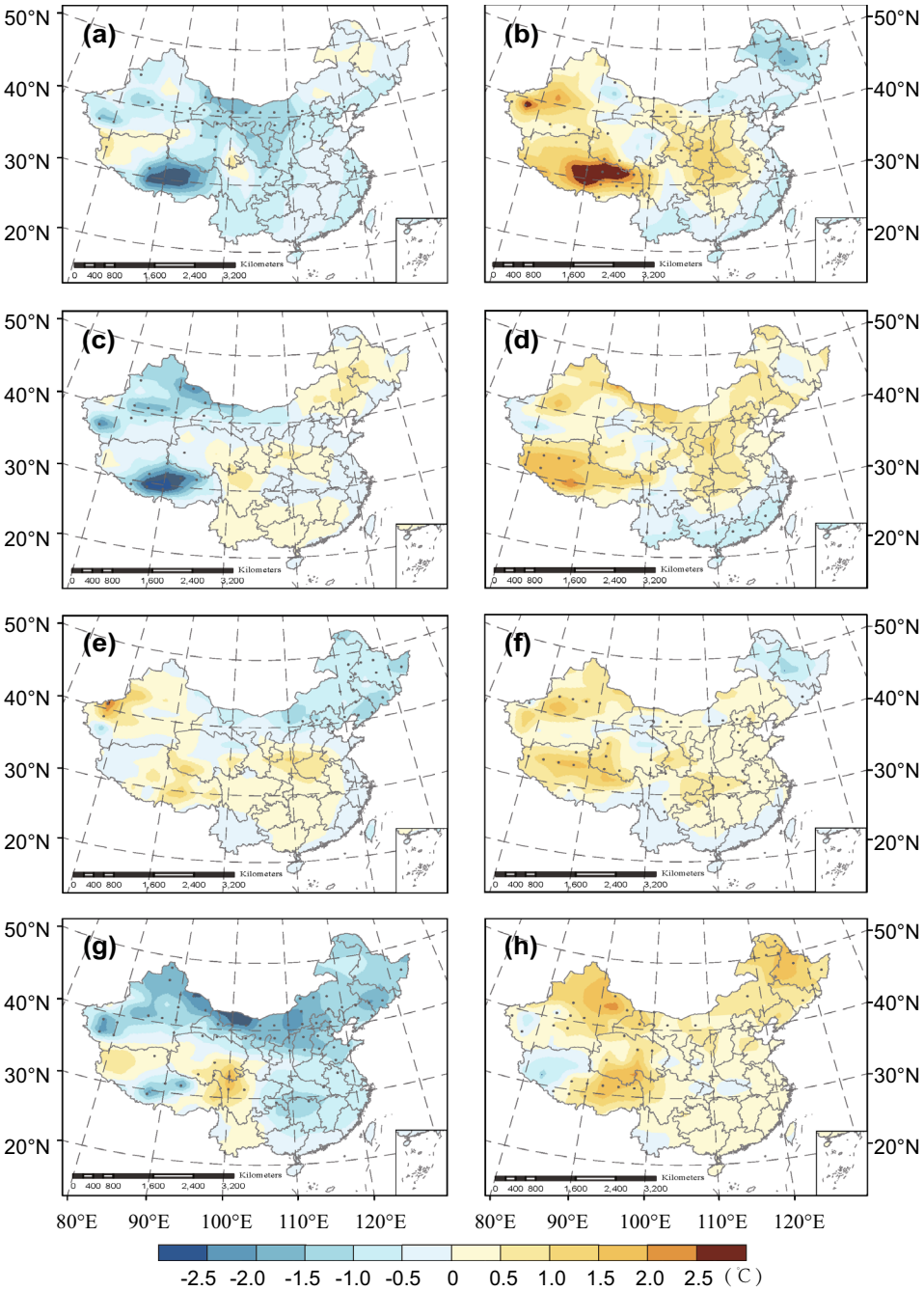

Fig. 6 Spatial patterns of average winter temperature anomalies between two post-volcanic winters and corresponding control experiment for China following large volcanic eruptions at tropical (**a**, **b**), low (**c**, **d**), mid (**e**, **f**), and high (**g**, **h**) latitudes in summer half-year (**a**, **c**, **e**, **g**) and winter half-year (**b**, **d**, **f**, **h**) by CESM. Dots indicate the confidence areas based on student *t* test

eastern China experienced a cold winter following summer tropical eruptions (Figs. 3a and 6a), and the Tibet was warm after winter tropical eruptions (Figs. 3b and 6b). Besides, the temperature patterns from observational data and simulation both showed that the temperature increased over all sub-regions of China after winter volcanic eruptions at high latitude (Figs. 3f and 6f).

The geopotential height fields at 500 hPa reveal the mechanism of how volcanic eruptions in different latitudinal zones affected the winter temperature pattern over China. Tropical eruptions in the summer half-year led to stronger Siberian High with 20 gpm anomalies, and developed East Asian trough with 20 gpm anomalies. The typical circulation field contributed to extensive cooling across China (Fig. 7a). Driven by tropical eruptions in the winter half-year, geopotential height anomalies over the Eurasian continent from north to south formed a "+-+" pattern. In addition, high pressure mainly covered western China. Thus, cold air was not easily transported to China (Fig. 7b). After eruptions at low latitude in the summer half-year, the enhanced polar vortex and decreased anomalies over the North Atlantic Ocean and east Asia produced a negative phase of AO.

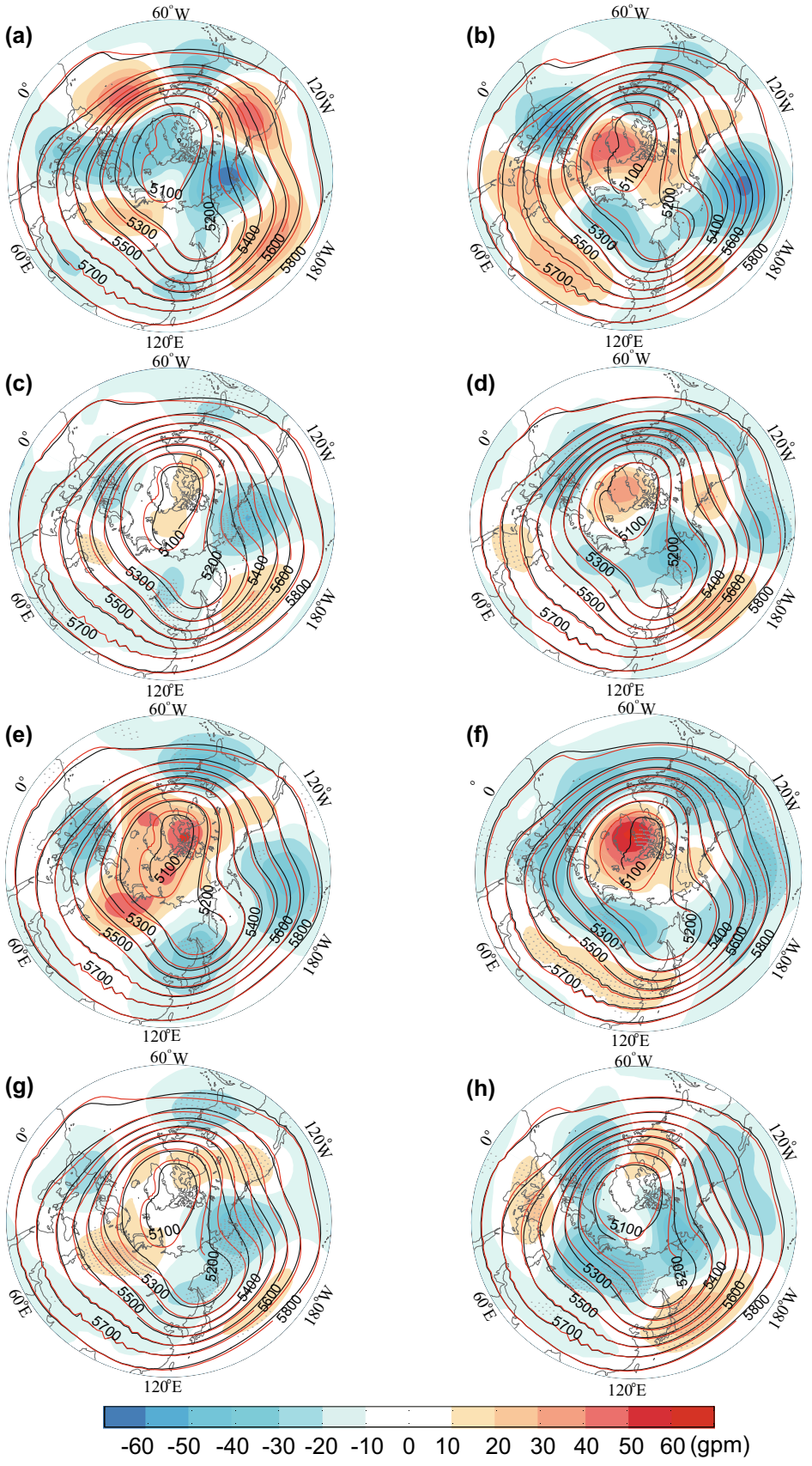

Fig. 7 Ensemble mean geopotential heights in 500 hPa of different volcanic forcings by CESM. The differences (shaded areas) were shown between two post-volcanic winters (red line) following large volcanic eruptions at tropical (**a**, **b**), low (**c**, **d**), mid (**e**, **f**), and high (**g**, **h**) latitudes in summer half-year (**a**, **c**, **e**, **g**) and winter half-year (**b**, **d**, **f**, **h**), with corresponding control experiment (black line). Dots indicate the confidence areas based on student *t* test

Since the geopotential height anomalies increased over the Caspian Sea and North Pacific, the East Asian trough was intensified and moved westward. This circulation blocked cold air transport to eastern China (Fig. 7c). The geopotential height anomalies greatly decreased from the Ural Mountains to Bering Strait and increased over the North Pacific following winter half-year eruptions at low latitude. This trend developed the zonal circulation and prevented cold air (Fig. 7d). Whether eruptions occurred in the summer or winter half-year, geopotential height patterns were similar after eruptions at mid-latitude. The positive anomaly with 60 gpm at the pole and negative anomalies with ov10–30 gpm mid latitude led to the negative phase of the AO, which contributed to the cooling over northeast. Furthermore, the East Asian trough after summer eruptions (Fig. 7e) was deeper than that after winter eruptions (Fig. 7f). Therefore, winter temperature decreased slightly over southeast coastal areas of China after summer eruptions. For eruptions at high latitude, the geopotential height pattern following summer eruptions (Fig. 7g) was similar to that after tropical eruptions (Fig. 7a). By contrast, geopotential height anomalies were anomalously low over the Siberian plain, and the East Asian trough was shallow after eruptions during the winter half-year (Fig. 7h), The pressure difference between high latitude and mid latitude increased, resulting in the positive phase of AO and extensive warming in China.

Generally, cooling over eastern China was mainly attributed to development of the East Asian trough and a high-pressure ridge near Lake Baikal. Moreover, the decrease of winter temperature in Tibet was dependent on the southern trough after large eruptions at tropical and low-mid latitudes. Cooling was induced by intensified zonal circulations after eruptions at high latitude.

4 Discussion

By comparing the above results with existing studies, this study highlights the effect of latitudinal location and season of large volcanic eruptions on temperature changes, using instrumental data. For example, Jia and Shi (2001) found that temperature decreased over Tibet and increased over southeast and northeast in the first month following seven large volcanic eruptions since 1956. Further, there was widespread cooling with a center over central China in the first year. Six of the seven volcanic events in Jia's study were at tropical and low latitudes. As an improvement, in our study, we increased the number of volcanic events to 29, and the sample size of tropical eruptions added up to 14. We focused on sequent winter temperature changes after eruptions. Specifically, the timespan was approximately 1 year between the first affected winter and eruptions in the summer half-year, which was only several months following eruptions in the winter half-year. When increasing the number of tropical volcanic events in our study, there was widespread cooling after summer eruptions and a warming and cooling spatial mosaic after winter eruptions. This suggests that the temperature response in China in our study is consistent with Jia's result.

Some studies have analyzed climate responses to volcanic forcing using climate modeling. For instance, using a time series of aerosol optical depth and the effective radius as volcanic forcing in the model, temperature responses to 21 large volcanic eruptions in eastern China were analyzed (Man et al. 2014). Zhang et al. (2013) selected volcanic eruptions without ENSO events during the two preceding winters and simulated temperature changes with weak or more intense variation of solar irradiance forcing, respectively. Miao et al. (2016) revealed the response of the East Asian winter monsoon to tropical volcanic eruptions using the Bergen Climate Model. The results showed obvious cooling in northern Xinjiang Province, central Inner Mongolia, and southern China in the third winter following 18 tropical eruptions. The cooling areas were similar to those in our research, in which winter temperature decreased considerably over the northern part of northwestern China and Hetao Plain after tropical summer eruptions. Although the above simulations were carried out during the last millennium (i.e., 800–2005 AD), the most involved number of volcanic eruptions was 21. It may be unable to investigate all types of eruptions as classified by location and season. Therefore, to solve this problem, we reconstructed the volcanic forcings, which were jointly identified by four eruption latitudes and two seasons. The results imply that both eruption latitude and season have an important effect on the spatial pattern of winter temperature over China.

In addition, our study presents several limitations that could introduce uncertainty. Due to the period of the instrumental temperature data is short, the sample size of volcanic events in each latitudinal zone was from 5 to 14 during the observational period. Although we can generalize a relationship between large eruptions at different latitudes and spatial patterns of winter temperature in China, the results have uncertainties, especially at low–mid latitude. Furthermore, none of the winter eruptions at high latitude were identified in the NCAR dataset. The winter volcanic forcing at high latitude in our simulation was constructed using summer volcanic forcing at the same latitude. This method could basically reproduce the intensity and duration of winter volcanic forcing at high latitude. Nevertheless, it may generate uncertainties. In addition, we removed the effect of ENSO on temperature changes over China following volcanic eruptions in this study. However, a large number of studies have found that large volcanic eruptions are likely to increase the probability of ENSO (Adams et al. 2003; McGregor and Timmermann 2011; Ohba et al. 2013). For

example, the proxy, such as tree-ring and ice core, shows that the probability of El Niño events increases in the year following volcanic eruptions (McGregor and Timmermann 2011). Besides, the simulation indicated that the stage of large tropical volcanic eruptions had significant influences on the ENSO evolution, which also leads to uncertainties. For example, there was a brief and weak La Niña-like response in the initial volcanic forcing stage, an El Niño-like response during the peak volcanic forcing stage, and in the declining volcanic forcing stage, the volcanic eruptions led to a La Niña-like response through the Bjerknes feedback (Wang et al. 2018). There are some studies on the response of ENSO to large volcanic eruptions with different latitudes using the Community Earth System Model Last Millennium Ensemble (CESM-LME) and reconstructed ENSO proxies (e.g., Liu et al. 2018; Zuo et al. 2018). The tropical and Northern Hemisphere eruptions can trigger an El Niño-like event within 2 years after the eruptions. Instead, a weak La Niña-like event tends to occur within 3 years after the Southern Hemisphere eruptions. Thus, the question arises as to whether the effects of Northern Hemisphere eruptions at different latitudes on ENSO occurrence and ENSO evolution are identical. Therefore, the response of ENSO to volcanic eruptions at various latitudes would be a potential direction to investigate spatial differences of temperature over China using the sensitivity experiments by CESM.

5 Conclusions

The spatial patterns of winter temperature in China were dependent on both volcanic season and latitudinal location. Following summer eruptions, winter temperature changes had great spatial variability. Nevertheless, there were widespread warmer winters occurred over most areas of China after winter eruptions.

The simulated regional winter temperature responses were very different following summer eruptions in four latitudinal zones. After tropical eruptions, the advance of barometric gradient between the equator and Arctic enhanced the Siberian High and East Asian trough, which led to winter temperature decreased about 0.4–1.6 °C over eastern China. However, because of a weakened Siberian High and Aleutian Low after eruptions at low latitude, winter temperature increased in eastern China, particularly in the northeast. The divergence of cold air over the Tibetan Plateau led to cooling in Tibet. After eruptions at mid-latitude, a typical pattern of trough–ridge–trough was seen over the Eurasian continent. The powerful blocking high extended southward to Lake Balkhash, which led to winter temperature decreased in northeast and increases in western China. In addition, there was strong cooling of 1.0–2.0 °C and 0.5–1.5 °C in the northwest and east-central China after eruptions at high latitude, respectively. It mainly depends on the intensified Siberian High and East Asian trough.

Although extensive warming over China was induced by winter eruptions regardless of volcano location, warming magnitudes and the dynamic mechanism were different by CESM. Following tropical eruptions, anomalous high pressure over East Asia could cut off the path of cold air and cause temperature increases of 1.0 °C over Tibet. The spatial response of winter temperature and atmospheric circulations following eruptions at low latitude was similar to that for eruptions at mid-latitude. The pressure gradient, which was higher in southern Eurasia than northern Eurasia, produced a southerly wind and contributed to slightly warming in most sub-regions of China. After eruptions at high latitude, the meridional circulation was weak and AO was in positive phase due to the geopotential height anomalies were significantly negative at high latitude. This generally increased winter temperature over China, particularly in the northeast and northwest. Thus, it is necessary to fully consider the potential influences of location and season for large volcanic eruptions when adapting to climate change induced by such eruptions.

Acknowledgements This work was supported by the National Natural Science Foundation of China (Grants 41831174 and 41671201), and the National Key Research and Development Project from Ministry of Science and Technology of China (Grant 2017YFA0603302).

References

Adams JB, Mann ME, Ammann CM (2003) Proxy evidence for an El Niño-like response to volcanic forcing. Nature 426(6964):274–278. https://doi.org/10.1038/nature02101

Casty C, Raible CC, Stocker TF, Wanner H, Luterbacher J (2007) A European pattern climatology 1766-2000. Clim Dyn 29(7–8):791–805. https://doi.org/10.1007/s00382-007-0257-6

Chang CP et al (2004) East Asian Monsoon. World Scientific Press, Singapore, pp 3–5

Chen W, Zhou Q (2012) Modulation of the Arctic oscillation and the East Asian winter climate relationships by the 11-year solar cycle. Adv Atmos Sci 29(2):217–226. https://doi.org/10.1007/s00376-011-1095-3

Cole-Dai J (2010) Volcanoes and climate. WIREs. Clim Change 1(6):824–839. https://doi.org/10.1002/wcc.76

Esper J et al (2013) European summer temperature response to annually dated volcanic eruptions over the past nine centuries. Bull Volcanol 75(7):736. https://doi.org/10.1007/s00445-013-0736-z

Fei J, Zhang ZH (2008) The AD1600 Huaynaputina eruption (peru) and climatic anomalies in the middle and lower reaches of the Yangtze River. Resour Environ Yangtze Basin 17(4):645–650 **(In Chinese)**

Fei J, Zhou J (2006) The possible climatic impact in China of Iceland's Eldgjá eruption inferred from historical sources. Clim Change 76(3):443–457. https://doi.org/10.1007/s10584-005-9012-3

Fischer EM, Luterbacher J, Zorita E, Tett SFB, Casty C, Wanner H (2007) European climate response to tropical volcanic eruptions over the last half millennium. Geophys Res Lett 34(5):306–316. https://doi.org/10.1029/2006GL027992

Gao CC, Robock A, Ammann C (2008) Volcanic forcing of climate over the past 1500 years: an improved ice core-based index for climate models. J Geophys Res Atmos 113(D23):D23111. https://doi.org/10.1029/2008JD010239

Ge QS, Zheng JY, Hao ZX, Shao XM, Wang WC, Luterbacher J (2010) Temperature variation through 2000 years in China: an uncertainty analysis of reconstruction and regional difference. Geophys Res Lett 37(3):L03703. https://doi.org/10.1029/2009GL041281

Gong DY, Wang SW, Zhu JH (2001) East Asian winter monsoon and Arctic oscillation. Geophys Res Lett 28(10):2073–2076. https://doi.org/10.1029/2000GL012311

Graf HF, Kirchner I, Robock A, Schult I (1993) Pinatubo eruption winter climate effects: model versus observations. Clim Dyn 9(2):81–93. https://doi.org/10.1007/BF00210011

Groisman PY (1992) Possible regional climate consequences of the Pinatubo eruption: an empirical approach. Geophys Res Lett 19(15):1603–1606. https://doi.org/10.1029/92GL01474

Huang RH, Chen JL, Huang G (2007) Characteristic's and variations of the East Asian monsoon system and its impacts on climate disasters in China. Adv Atmos Sci 24(6):993–1023. https://doi.org/10.1007/s00376-007-0993-x

Hurrell JW et al (2013) The community earth system model: a framework for collaborative research. Bull Am Meteor Soc 94(9):1339–1360. https://doi.org/10.1175/BAMS-D-12-00121.1

Iles CE, Hegerl GC, Schurer AP, Zhang XB (2013) The effect of volcanic eruptions on global precipitation. J Geophys Res 118(16):8770–8786. https://doi.org/10.1002/jgrd.50678

Jia PQ, Shi GY (2001) Study on the effects of volcanic eruption and solar activity on climate in China in recent 50 years. Plat Meteorol 20(3):225–233 **(In Chinese)**

Kirchner I, Stenchikov GL, Graf HF, Robock A, Antuna JC (1999) Climate model simulation of winter warming and summer cooling following the 1991 Mount Pinatubo volcanic eruption. J Geophys Res 104(D16):19039–19055. https://doi.org/10.1029/1999JD900213

Kravitz B, Robock A (2011) Climate effects of high-latitude volcanic eruptions: role of the time of year. J Geophys Res 116(D1):D01105. https://doi.org/10.1029/2010JD014448

Lamarque JF et al (2012) CAM-chem: description and evaluation of interactive atmospheric chemistry in the community earth system model. Geosci Model Dev 5(2):369–411. https://doi.org/10.5194/gmd-5-369-2012

Landrum L, Otto-Bliesner BL, Wahl ER, Conley A, Lawrence PJ, Rosenbloom N, Teng HY (2013) Last millennium climate and its variability in CCSM4. J Clim 26(4):1085–1111. https://doi.org/10.1175/JCLI-D-11-00326.1

Lehner F, Joos F, Raible CC, Mignot J, Born A, Keller KM, Stocker TF (2015) Climate and carbon cycle dynamics in a CESM simulation from 850 to 2100 CE. Earth Syst Dyn 6(2):411–434. https://doi.org/10.5194/esd-6-411-2015

Lim HG, Yeh SW, Kug JS, Park YG, Park JH, Park R, Song CK (2015) Threshold of the volcanic forcing that leads the El Niño-like warming in the last millennium: results from the ERIK simulation. Clim Dyn 46(11–12):3725–3736. https://doi.org/10.1007/s00382-015-2799-3

Liu F, Chai J, Wang B, Liu J, Zhang X, Wang ZY (2016) Global monsoon precipitation responses to large volcanic eruptions. Sci Rep 6(1):24331. https://doi.org/10.1038/srep24331

Liu F, Li JB, Wang B, Liu J, Li T, Huang G, Wang ZY (2018) Divergent El Niño responses to volcanic eruptions at different latitudes over the past millennium. Clim Dyn 50(9–10):3799–3812. https://doi.org/10.1007/s00382-017-3846-z

Luterbacher J, Pfister C (2015) The year without a summer. Nat Geosci 8(4):246–248. https://doi.org/10.1038/ngeo2404

Man WM, Zhou TJ, Jungclaus JH (2014) Effects of large volcanic eruptions on global summer climate and East Asian monsoon changes during the last millennium: analysis of MPI-ESM simulations. J Clim 27(19):7394–7409. https://doi.org/10.1175/JCLI-D-13-00739.1

McGregor S, Timmermann A (2011) The effect of explosive tropical volcanism on ENSO. J Clim 24(8):2178–2191. https://doi.org/10.1175/2010JCLI3990.1

Miao JP, Wang T, Zhu YL, Min JZ, Wang HJ, Guo D (2016) Response of the East Asian winter monsoon to strong tropical volcanic eruptions. J Clim 29(13):5041–5057. https://doi.org/10.1175/JCLI-D-15-0600.1

Neely RR, Conley AJ, Vitt F, Lamarque JF (2016) A consistent prescription of stratospheric aerosol for both radiation and chemistry in the community earth system model (CESM1). Geosci Model Dev 9(7):2459–2470. https://doi.org/10.5194/gmd-9-2459-2016

Newhall C, Self S, Robock A (2018) Anticipating future Volcanic Explosivity Index (VEI) 7 eruptions and their chilling impacts. Geosphere 14(2):572–603. https://doi.org/10.1130/GES01513.1

Ohba M, Shiogama H, Yokohata T, Watanabe M (2013) Impact of strong tropical volcanic eruptions on ENSO simulated in a coupled GCM. J Clim 26(14):5169–5182. https://doi.org/10.1175/JCLI-D-12-00471.1

Oman L, Robock A, Stenchikov G, Schmidt GA, Ruedy R (2005) Climatic response to high-latitude volcanic eruptions. J Geophys Res 110(D13):2515–2530. https://doi.org/10.1029/2004JD005487

Ottera OH (2008) Simulating the effects of the 1991 Mount Pinatubo volcanic eruption using the ARPEGE atmosphere general circulation model. Adv Atmos Sci 25(2):213–226. https://doi.org/10.1007/s00376-008-0213-3

Parker DE, Wilson H, Jones PD, Christy JR, Folland CK (1996) The impact of Mount Pinatubo on world-wide temperatures. Int J Climatol 16(5):487–497. https://doi.org/10.1002/(SICI)1097-0088(199605)16:5%3c487:AID-JOC39%3e3.0.CO;2-J

Predybaylo E, Stenchikov GL, Wittenberg AT, Zeng FR (2017) Impacts of a Pinatubo-size volcanic eruption on ENSO. J Geophys Res 122(2):925–947. https://doi.org/10.1002/2016JD025796

Robock A (2000) Volcanic eruptions and climate. Rev Geophys 38(2):191–219. https://doi.org/10.1029/1998RG000054

Robock A, Free MP (1996) The volcanic record in ice cores for the past 2000 years. Springer, New York, pp 533–546

Robock A, Mao J (1992) Winter warming from large volcanic eruptions. Geophys Res Lett 19(24):2405–2408. https://doi.org/10.1029/92GL02627

Robock A, Mao J (1995) The volcanic signal in surface temperature observations. J Clim 8(5):1086–1103. https://doi.org/10.1175/1520-0442(1995)008%3c1086:TVSIST%3e2.0.CO;2

Schneider DP, Ammann CM, Otto-Bliesner BL, Kaufman DS (2009) Climate response to large, high-latitude and low-latitude volcanic eruptions in the community climate system model. J Geophys Res 114(D15):D15101. https://doi.org/10.1029/2008JD011222

Shindell DT, Schmidt GA, Mann ME, Faluvegi G (2004) Dynamic winter climate response to large tropical volcanic eruptions since 1600. J Geophys Res 109(D5):D05104. https://doi.org/10.1029/2003JD004151

Stevenson S, Otto-Bliesner B, Fasullo J, Brady E (2016) "El Niño like'' hydroclimate responses to last millennium volcanic eruptions. J Clim 29(8):2907–2921. https://doi.org/10.1175/JCLI-D-15-0239.1

Stevenson S, Fasullo JT, Otto-Bliesner BL, Tomas RA, Gao CC (2017) Role of eruption season in reconciling model and proxy responses to tropical volcanism. P Natl Acad Sci USA 114(8):1822–1826. https://doi.org/10.1073/pnas.1612505114

Wang B (2006) The Asian monsoon. Springer, New York, pp 89–95

Wang L, Chen W (2010) How well do existing indices measure the strength of the East Asian winter monsoon? Adv Atmos Sci 27(4):855–870. https://doi.org/10.1007/s00376-009-9094-3

Wang T, Guo D, Gao Y, Wang H, Zheng F, Zhu Y, Miao JP, Hu YY (2018) Modulation of ENSO evolution by strong tropical volcanic eruptions. Clim Dyn 51(7–8):2433–2453. https://doi.org/10.1007/s00382-017-4021-2

Xu Q (1986) The abnormal weather of China for summer 1980 and its relationship with the volcanic eruptions of St. Helens. Acta Meteorol Sin 44(4):426–432

Xu Q (1995) Influences of Pinatubo volcanic clouds on large scale climate in 1992. Q J Appl Meteorol 6(1):35–42 **(In Chinese)**

Zhang D, Blender R, Fraedrich K (2013) Volcanoes and ENSO in millennium simulations: global impacts and regional reconstructions in East Asia. Theor Appl Climatol 111(3–4):437–454. https://doi.org/10.1007/s00704-012-0670-6

Zhang XZ, Wu MW, Liu Y, Hao ZX, Zheng JY (2018) The relationship between the East Asian summer monsoon and El Niño-Southern Oscillation revealed by reconstructions and a control simulation for millennium. Quat Int 493:106–113. https://doi.org/10.1016/j.quaint.2018.06.024

Zheng JY, Wu MW, Ge QS, Hao ZX, Zhang XZ (2017) Observed, reconstructed, and simulated decadal variability of summer precipitation over eastern China. J Meteorol Res 31(1):49–60. https://doi.org/10.1007/s13351-017-6115-5

Zhou Q, Chen W, Zhou W (2013) Solar cycle modulation of the ENSO impact on the winter climate of East Asia. J Geophys Res 118(11):5111–5119. https://doi.org/10.1002/jgrd.50453

Zuo M, Man WM, Zhou TJ, Guo Z (2018) Different impacts of northern, tropical, and southern volcanic eruptions on the tropical Pacific SST in the last millennium. J Clim 31(17):6729–6744. https://doi.org/10.1175/JCLI-D-17-0571.1